Endochondral bone in an Early Devonian 'placoderm' from Mongolia

Martin D. Brazeau[1,2], Sam Giles [2,3,4], Richard P. Dearden[1,5], Anna Jerve[1,6], Y.A. Ariunchimeg[7], E. Zorig[8], Robert Sansom[9], Thomas Guillerme[10], Marco Castiello[1]

[1] *Department of Life Sciences, Imperial College London, Silwood Park Campus, Buckhurst Rd, Ascot, SL5 7PY, UK;*

[2] *Department of Earth Sciences, Natural History Museum, Cromwell Road, London SW7 5BD, UK;*

[3] *School of Geography, Earth and Environmental Sciences, University of Birmingham, Birmingham, UK;*

[4] *Department of Earth Sciences, University of Oxford, South Parks Road, Oxford, OX1 3AN, UK;*

[5] *CR2P Centre de Recherche en Paléontologie – Paris, Muséum national d'Histoire naturelle, Sorbonne Universités, CNRS, CP 38, 57 Rue Cuvier, 75231, Paris, Cedex 05, France*

[6] *Department of Organismal Biology, Subdepartment of Evolution and Development, Uppsala University, Norbyvägen 18A, 752 36 Uppsala, Sweden;*

[7] *Natural History Museum, P.O. Box 46/52, Ulaanbaatar 1420, Mongolia*

[8] *Institute of Paleontology, Mongolian Academy of Science, P.O. Box 46/650, S. Danzan Street 3/1, Chingeltei District. Ulaanbaatar 15160, Mongolia;*

[9] *School of Earth and Environmental Sciences, University of Manchester, Manchester M13 9PT, UK;*

[10] *Department of Animal and Plant Sciences, The University of Sheffield, Sheffield S10 2TN, UK;*

Endochondral bone is the main internal skeletal tissue of nearly all osteichthyans[1,2] — the group comprising more than 60,000 living species of bony fishes and tetrapods. Chondrichthyans (sharks and their kin) are the living sister group of osteichthyans and have cartilaginous endoskeletons, long considered the ancestral condition for all jawed vertebrates (gnathostomes)[3,4]. The absence of bone in modern jawless fishes and the absence of endochondral ossification in early fossil gnathostomes appears to lend support to this conclusion. Here we report the discovery of extensive endochondral bone in a new genus of 'placoderm'-like fish from the Early Devonian (Pragian) of western Mongolia described using x-ray computed microtomography (XR-µCT). The fossil consists of a partial skull roof and braincase with anatomical details providing strong evidence of placement in the gnathostome stem group. However, its endochondral space is filled with an extensive network of fine trabeculae resembling the endochondral bone of osteichthyans. Phylogenetic analyses place this new taxon as a proximate sister group of the gnathostome crown. These results provide direct support for theories of generalised bone loss in chondrichthyans[5,6]. Furthermore, they revive theories of a phylogenetically deeper origin of endochondral bone and its absence in chondrichthyans as a secondary condition[7,8].

Systematic palaeontology

Placodermi M'Coy 1848

Minjinia turgenensis gen. et sp. nov.

Etymology. Generic name honours the memory of Chuluun Minjin for his extensive contributions to the Palaeozoic stratigraphy of Mongolia, his enthusiastic support of this work, and introducing us to the Yamaat River locality. Specific name recognises the provenance of the fossil from the Turgen region, Uvs aimag of western Mongolia.

Holotype. Institute of Paleontology, Mongolian Academy of Sciences MPC-FH100/9.1, a partial braincase and skull roof.

Type locality. Turgen Strictly Protected Area, Uvs province, western Mongolia; near the top of the stratigraphic sequence that occurs between the Tsagaan-Salaat and Yamaat Rivers.

Formation and age. Upper part of Tsagaansalaat Formation, Pragian (Early Devonian)[9,10].

Diagnosis. 'placoderm'-grade stem gnathostome with endochondral bone, deep epaxial muscle cavities flanking a slender occipital ridge, and the following possible autapomorphies: dermal bones covered in sparsely placed tubercles, penultimate spino-occipital nerve canal substantially larger in diameter than others.

Description

MPC-FH100/9.1 consists of a partial braincase and skull roof (Fig. 1). The skull roof is ornamented with sparsely distributed stellate tubercles resembling those of the Siberian 'placoderm' *Dolganosteus*[11]. Towards the midline of the skull roof, the tubercles are larger and more pointed, and are more broadly separated from each other by unornamented fields. The specimen shows signs of extensive post-mortem transport, with angles of the braincase worn off and much of the skull roof and some of the braincase preserved as a mould. Individual skull roof ossifications cannot be identified, although this may be due to the dominantly mouldic preservation. There appears to have been a prominent nuchal plate eminence comparable to acanthothoracids[12-14].

Endoskeletal tissue. The braincase of MPC-FH100/9.1 is well ossified, comprising an external bony sheath filled with an extensive matrix of spongy tissue (Fig. 2a-b; Extended Data Fig. 1; Supplementary Videos 1 & 2). The trabecles forming this tissue are irregular and branching, less than 1mm thick and often curved, and resemble most closely the endochondral tissue of osteichthyans (Fig. 2c-d). As such, we interpret this as endochondral bone. Notably, this is found in all preserved regions of the braincase, in contrast to the isolated trabeculae identified as endochondral bone in *Boreaspis*[15] and *Bothriolepis*[16]. The margins of the braincase, the endocranial walls, and the boundaries of nerve and blood canals, are formed from a thicker tissue which we interpret as perichondral bone. This suggests that the endoskeleton of *Minjinia* comprises osteichthyan-like endochondral bone, with an ossified perichondrium. To address the possible alternative explanation that it is an aberrant instance of calcified cartilage, we compared the structure of this tissue with rarely-preserved mineralized cartilage in the stem chondrichthyan *Diplacanthus crassismus* (National Museums of Scotland specimen NMS 1891.92.334; Fig. 2e-f) observed using synchrotron tomography. The cancellae within the endochondral tissue of *Minjinia* are irregular, with a diameter of approximately 1-2mm. This tissue is distinctly unlike the

calcified cartilage of *Diplacanthus* in appearance, which consists of a densely packed matrix of irregularly stacked chondrons between 20-60 μm in diameter.

Neurocranium. The braincase is preserved from the level of the right posterior orbital wall to the posterior end of the occipital ridge. Occipital glenoid condyles are not preserved, but broad, flat parachordal plates are present, separated by a midline groove that accommodated a relatively narrow notochordal tunnel. A transverse fissure spans the basicranial surface at about mid-length of the preserved portion. It clearly demarcates the anterior margin of the parachordal plates and may correspond to the ventral cranial fissure of crown-group gnathostomes. However, unlike in crown gnathostomes, it is traversed by a substantial anterior extension of the cranial notochord. The courses of the lateral dorsal aortae are marked by a pair of sulci on the lateral margins of the parachordal plates. A narrow, shallow sulcus for the efferent hyoid artery is present on the preserved right side of the specimen, immediately behind the level of the orbit (Fig. 1a).

The lateral surface of the braincase is preserved on the right side as a mouldic impression in the matrix (Fig. 1). A sharply demarcated hyoid fossa is present on the lateral wall of the otic region (Fig. 1). Posterior to this, a stout but pronounced vagal process with a pair of rounded eminences likely corresponds to the branchial arch articulations. There is no evidence for a pair of anterior and posterior divisions to the vagal process, which are typically seen in other 'placoderms'. A well-developed 'placoderm'-like craniospinal process is absent; its homologous position is instead covered in perichondral bone and marked by a low ridge (Fig. 1).

In posterior view, a tall, narrow median otic ridge is evident and resembles the morphology of *Romundina*[17] and *Arabosteus*[18]. Similar to these taxa, the median otic ridge is flanked by two large occipital fossae for the epaxial musculature. The notochordal tunnel is approximately the same size as or smaller than the foramen magnum, as in 'placoderms' and in contrast with crown-group gnathostomes. A metotic fissure is absent.

Endocast. A partial cranial endocast is preserved, consisting of the hindbrain cavity, partial midbrain cavity, labyrinth cavities, and posteromedial corner of the orbital region. The two primary trunk canals of the trigeminal nerve ($N.V_1$ and $N.V_{2,3}$) are preserved (Fig. 1; Extended Data Fig. 2). The acoustic (N.VIII) and facial nerve (N.VII) canals share a common trunk canal behind the trigeminal nerves, as in many other 'placoderms' [17,19-21]. The supraopthalmic branch opens into the rear wall of the orbit and part of its supraorbital course

is preserved (Extended Data Figs. 2, 3). A slender branch extends below the labyrinth and divides into palatine and hyomandibular branches (Extended Data Figs. 2, 3). As in other 'placoderm'-grade taxa, the vagus nerve (N. X) trunk canal is very large in diameter and exits from immediately behind the labyrinth cavity (Fig. 1; Extended Data Fig. 2). The spino-occipital region resembles other 'placoderms' in being extended. At least four spino-occipital nerve canals are present in a linear series, and the penultimate canal is largest in diameter (Fig. 1; Extended Data Fig. 2). Intercalating these is a network of occipital artery canals branching from the dorsal aortae.

The skeletal labyrinth is not complete on either side of the specimen, but can mostly be reconstructed according to the assumption of bilateral symmetry. The most significant feature is that the labyrinth and endolymphatic cavity are joined to the main endocavity chamber (Fig. 1). This is a striking contrast to other 'placoderms' and closely resembles crown-group gnathostomes[22]. The endolymphatic canals are elongate and tubular, extending posterolaterally to reach the skull roof, though external openings cannot be clearly identified. The anterior semi-circular canal follows the saccular cavity closely as in petalichthyids[23](Fig. 1; Extended Data Fig. 2). However, the horizontal and posterior canals appear to extend well away from the saccular chamber (Fig. 1, Extended Data Fig. 2). The dorsal junctions of the anterior and posterior canals are joined in a crus commune, as in *Romundina*[17] and *Jagorina*[19]. A sinus superior is absent.

Phylogenetic analyses

We conducted phylogenetic analyses under four different protocols: equal weights parsimony, implied weights parsimony, an unpartitioned Bayesian analysis, and a Bayesian analysis with characters partitioned by fit determined under implied weights parsimony[24] (see Extended Data Figs. 4-7). All phylogenetic analyses consistently place *Minjinia* as a stem-group gnathostome, proximate to the gnathostome crown (Fig. 3, Extended Data Figs 4,5). Equal weights parsimony recovers *Minjinia* in a position crownward of arthrodires but outside of a grade consisting of *Entelognathus*, *Ramirosuarezia*, and *Janusiscus*. Under implied weights, these three taxa move onto the osteichthyan stem and *Minjinia* is placed as the immediate sister taxon of the gnathostome crown. Under Bayesian analyses, arthrodires are resolved as more crownward than *Minjinia.* However, the latter analyses fail to recover arthrodires as a clade and the node uniting them with the crown to the exclusion of *Minjinia* is extremely weakly supported (posterior probability: 0.52-0.55). Under parsimony, the crownward position of *Minjinia* is unambiguously supported by the skeletal labyrinth and

endolymphatic duct being confluent with the main cranial cavity[22] (Fig. 3). In common with arthrodires and the gnathostome crown, *Minjinia* possesses a division of the facial nerve deep to the transverse otic process (Fig. 1; Extended Data Fig. 2). However, *Minjinia* is excluded from the gnathostome crown group due to the absence of a metotic fissure and a posterior dorsal fontanelle, and presence of broad, flat parachordal plates expanded behind the saccular cavity (Fig. 3, Supplementary Information).

We undertook ancestral states reconstructions to assess the evolutionary history of endochondral bone (Fig. 3, Extended Data Figs. 6 & 7). Interestingly, parsimony analysis fails to recover secondary homology of this trait between *Minjinia* and osteichthyans. The crownward placement of *Minjinia* is, in fact, based on independent evidence relating to anatomical features of the braincase and endocast. However, the strict precision of parsimony reconstructions makes it insensitive to underlying uncertainty. To explore this, we used likelihood reconstructions and compared the ancestral state reconstructions under equal rates (ER) and all rates different (ARD) variants of the Mkv model on branch-length-rescaled parsimony trees and Bayesian trees. On the parsimony trees, both models show substantial non-zero probabilities (0.23 for ER; 0.39 for ARD; Extended Data Table 1) for the presence of endochondral bone in the common node of *Minjinia* and Osteichthyes (Extended Data Fig. 6) in the parsimony trees. The ARD model shows the best likelihood score and a better AIC fit for endochondral bone (Extended Data Table 1), favouring repeated losses of this tissue over multiple gains (see Discussion). The values are substantially lower in the Bayesian trees (Extended Data Fig. 7, Extended Data Table 1), but this results from the relative positions of *Minjinia* and arthordires, which is not well supported in those trees.

Discussion

Minjinia presents an unusual discovery of extensive endochondral bone in a 'placoderm'-grade fish, with repercussions for the phylogenetic origin of this tissue and the problem of early gnathostome relationships more generally. The vertebrate skeleton is split into two systems: the exoskeleton (external achondral dermal bones) and endoskeleton (internal chondral bones) [1]. Dermal bone evolved at least 450 million years ago in jawless stem gnathostomes, but the endoskeleton in these taxa is not endochondrally ossified (but see below). More crownward stem gnathostomes (osteostracans and 'placoderms') surround their cartilaginous endoskeleton in a sheath of perichondral bone. Extant chondrichthyans lack both dermal and perichondral bone, possessing a cartilaginous endoskeleton enveloped by prismatic calcified cartilage. Endochondral bone, in which the cartilaginous endoskeletal

precursor is invaded by and eventually replaced by bone, is widely considered an osteichthyan apomorphy based on clear prior polarity[3,7,25,26]. However, recent work has cast doubt on this assertion. The recognition that dermal bone is secondarily lost in chondrichthyans[27,28] is consonant with prior knowledge of the loss of perichondral bone in this same lineage [29]. Taken together, this has revived uncertainty about the true phylogenetic timing of the origin of endochondral ossification[8].

Minjinia does not represent the first report of endochondral bone outside of Osteichthyes. However, it is by far the most extensive and unequivocal example, and raises explicit questions in light of the proximity of *Minjinia* to the gnathostome crown. Isolated examples of trabecular bone, typically restricted to a small region of the neurocranium, have historically been reported in boreaspid osteostracans[15,30], buchanosteid arthrodires[31] and petalichthyids[32]. However, these reports have all been dismissed as misidentifications[26], possibly representing the retreat of perichondral bone deposited during cartilage growth[33]. Most recently, trabeculae in supposed endoskeletal bones of *Bothriolepis* have been termed endochondral bone[16], although the small scale of these is in line with 'superficial' perichondral trabeculae seen elsewhere. In line with ref. 26, we found no evidence of endochondral bone in material of *Buchanosteus* held in the Natural History Museum, London, or indeed in any other 'placoderms' we have examined. The *Epipetalichthys* holotype (Museum für Naturkunde, Berlin specimen MB.f.132.1-3) shows an apparently spongiose infilling in the anterior region of the braincase, but the identity of this structure, or even whether it is biological, cannot be determined.

Does endochondral bone have a deep origin within the gnathostome stem group? This would imply repeated losses of this tissue. We do find some statistical support for this hypothesis (Fig. 3, Extended Data Figs. 6, 7; Extended Data Table 1), and the model is well justified on prior phylogenetic and biological grounds. Endochondral bone has long been known to be inconsistently developed across 'primitive' bony fishes: incomplete or entirely absent ossification of the endoskeleton is known in both Palaeozoic actinopterygians[34] and sarcopterygians[35], as well as more recent taxa[36]. The frequent absence of endochondral bone is considered secondary, and other controlling factors such as body size, maturity, mechanical stress, and buoyancy can determine its degree of development[1]. Our findings are also in agreement with studies establishing a genetic basis for secondary loss of all bone types within chondrichthyans[5,37,38], with the failure to produce endochondral bone likely representing arrested development of chondrocytes as opposed to a primary lack of ability[6].

Another confounding factor in this question is the problem of 'placoderm' relationships. Although currently resolved as a deeply pectinate grade along the gnathostome stem, the backbone of this arrangement has poor statistical support and there is a lack of consistency in the arrangement of plesia. *Minjinia* itself highlights this uncertainty, given its highly unexpected character combinations. Notwithstanding its endochondral bone and crown-gnathostome-like inner ear structure, it strongly resembles 'acanthothoracids'—the 'placoderms' widely considered among the most removed from the gnathostome crown (i.e. most 'primitive'). This apparent character conflict could perhaps be more easily reconciled with a more coherent (though not necessarily monophyletic) 'placoderm' assemblage. Indeed, the highly pectinate structure of the 'placoderm' grade seems symptomatic of an overemphasis on characters and taxa resembling the crown group, thereby undersampling characters that could stabilise a clear picture of 'placoderm' interrelationships.

Minjinia reveals new data on 'placoderm' endoskeleton and tissue diversity from Mongolia—an otherwise extremely poorly known biogeographic realm for early gnathostomes. The phylogenetic placement of this 'acanthothoracid'-like taxon crownward of all non-maxillate 'placoderms', in conjunction with possession of extensive endochondral bone, highlights the importance of material from traditionally undersampled geographic areas. The presence of endochondral bone renews the hypothesis that this tissue is evolutionarily ancient and was lost secondarily in chondrichthyans[7,8]. This view is overall consistent with evidence of generalised bone loss in chondrichthyans, potentially as a result of the suppression of bone-generating molecular genetic pathways[6,38]. Continued work in Mongolia and re-evaluation of phylogenetic datasets will be necessary to address this, with the results likely to lead to substantial re-evaluation of gnathostome phylogeny.

Acknowledgements. M. Bolortsetseg generously assisted MDB with contacts and field experience in Mongolia. Fieldwork was supported by National Geographic Society grants CRE 8769-10 and GEFNE35-12 to MDB. ALJ's field contributions were supported by funds from the Anna Maria Lundin's stipend from Smålands Nation, Uppsala University. RS's field contributions were supported by a Royal Society Research Grant and the University of Manchester. The majority of this work was supported by the European Research Council (ERC) under the European Union's Seventh Framework Programme (FP/2007-2013)/ERC Grant Agreement number 311092 to MDB. RPD was also supported by the Île-de-France DIM (domaine d'intérêt majeur) matériaux anciens et patrimoniaux grant PHARE. Stig Walsh is thanked for access and loan of specimen at the National Museums of Scotland.

Synchrotron tomography was performed at the ESRF (application LS 2451) with the assistance of Paul Tafforeau. SG was supported by a Royal Society Dorothy Hodgkin Research Fellowship. Matt Friedman is thanked for undertaking the X-ray computed microtomography analysis. TNT was made available with the support of the Willi Hennig Society.

Author Contributions: MDB conceived and designed the study. MDB, AJ, YAA, and EZ participated in all field seasons. RPD and AJ undertook preliminary CT scanning and segmentation that revealed the fossil was a 'placoderm' and had endochondral bone. RS discovered the first vertebrate remains in the first field season at Yamaat Gol in 2010. SG did most of the segmentation of *Minjinia* with input from MDB. AJ performed segmentation of *Diplacanthus* tissue. MC provided input on occipital comparative morphology of 'placoderms'. RPD provided data and comparative analyses and data for endoskeletal tissue. YAA provided background on the geology, palaeontology, and stratigraphy of the type location; EZ and YAA organized field logistics and permitting. MDB, SG, MC, RPD, and AJ undertook the anatomical interpretation and prepared the figures. MDB and SG conducted the phylogenetic analyses. RS conducted the parsimony branch support analyses. TG wrote the script for generating MrBayes partitions from TNT's character fits table and conducted the likelihood and model-fitting analyses. The manuscript was written by MDB, RPD, and SG.

Author Information:

Correspondence and requests for materials should be addressed to m.brazeau@imperial.ac.uk.

Methods

X-ray computed microtomography. We scanned MPC-FH100/9.1 using the Nikon XT 225s at the Museum of Paleontology, University of Michigan with the following parameters: 200kV, 140μA, over 3123 projections and a voxel size of 32.92μm. We conducted segmentation using Mimics 19.0 (http://biomedical.materialise.com/mimics; Materialise, Leuven, Belgium) and we imaged models for publication using Blender (https://www.blender.org).

Synchrotron light propagation phase contrast tomography. We imaged *Diplacanthus crassismus* specimen NMS 1891.92.334 on Beamline 19 of the European Synchrotron Radiation Facility, using propagation phase-contrast synchrotron microtomography. We performed a spot scan with an energy of 116keV, achieving a voxel size of 0.55 μm. We processed the resulting tomograms using VG StudioMax 2.2 (Volume Graphics, Germany), and prepared images in Blender.

Phylogenetic analysis. We conducted a parsimony analysis using TNT 1.5 [39] and Bayesian analysis using MrBayes v 3.2.7[40]. The dataset consisted of 95 taxa and 284 discrete characters based on a pre-existing dataset[41]. We employed Osteostraci and Galeaspida as composite outgroups. We conducted parsimony analysis using both equal weights and implied weights methods. Global settings were 1000 search replicates and a hold of up to 1 million trees. Equal weights parsimony analyses were conducted using the ratchet with default settings. Implied weights parsimony used a concavity parameter of 3 and the search was without the ratchet. Command lists are included in Supplementary Information. We conducted Bayesian analysis using both a partitioned and unpartitioned dataset. We used the Mkv model [42] and gamma rate distribution. We ran the analyses for 5 million generations with a relative burn-in fraction of 0.25. Runs were checked for convergence using Tracer[43]. We partitioned the dataset using a newly proposed method[24] that partitions the data according to homoplasy levels. Using the results of implied weights parsimony conducted in TNT, we created a text table of character fit values. We wrote an R[44] script to generate a list of partition commands for MrBayes. To reduce the number of partitions with small numbers of characters, we concatenated the partitions by rounding the fitness scores to 2 significant figures, yielding 10 individual partitions.

We assessed parsimony ancestral states visually using Mesquite[45]. Likelihood and Bayesian ancestral states were estimated in R using the castor package[46]. Prior to calculating likelihood ancestral states on parsimony trees, we scaled branch lengths using PAUP*[47] and calculated the likelihood scores for all of the trees under the Mkv model. The trees were then exported with branch lengths. To account for overall uncertainty in tree estimates, we estimated ancestral states on 100 trees randomly selected from the fundamental set of most parsimonious trees and two times 50 trees selected from the 75% last trees of each posterior tree distribution from the Bayesian analysis. We then run an ancestral states estimation Mk model (using the castor R package) using both the Equal Rates (ER) and All Rates Different (ARD) models. This resulted in 400 ancestral states estimations. For each estimation we extracted the overlap log likelihood, the AIC (counting one parameter for the ER model and

two for the ARD model) and the scaled log likelihood (probability) for the presence and absence of the endochondral bone character (character 4) for the last common node of *Minjinia* and crown-group gnathostomes. We present the median value of these distributions of the estimations overall log likelihoods, AICs and presence or absence of endochondral bone in Extended Data Table 1.

Data availability

The holotype specimen of *Minjinia turgenensis* will be permanently deposited in the collections of the Institute of Paleontology, Mongolian Academy of Sciences. Original tomograms are available at (doi:10.6084/m9.figshare.12301229) and rendered models are available at (doi:10.6084/m9.figshare.12301223). The phylogenetic character list and dataset are available as Supplementary Information S1 and S2. The LifeScience Identifier for *Minjinia turgenensis* is urn:lsid:zoobank.org:act:82A1CEEC-B990-47FF-927A-D2F0B59AEA87

Code availability

R code for generating partitions based on character fits and code for likelihood ancestral states reconstructions and plots are available in the Supplementary Information.

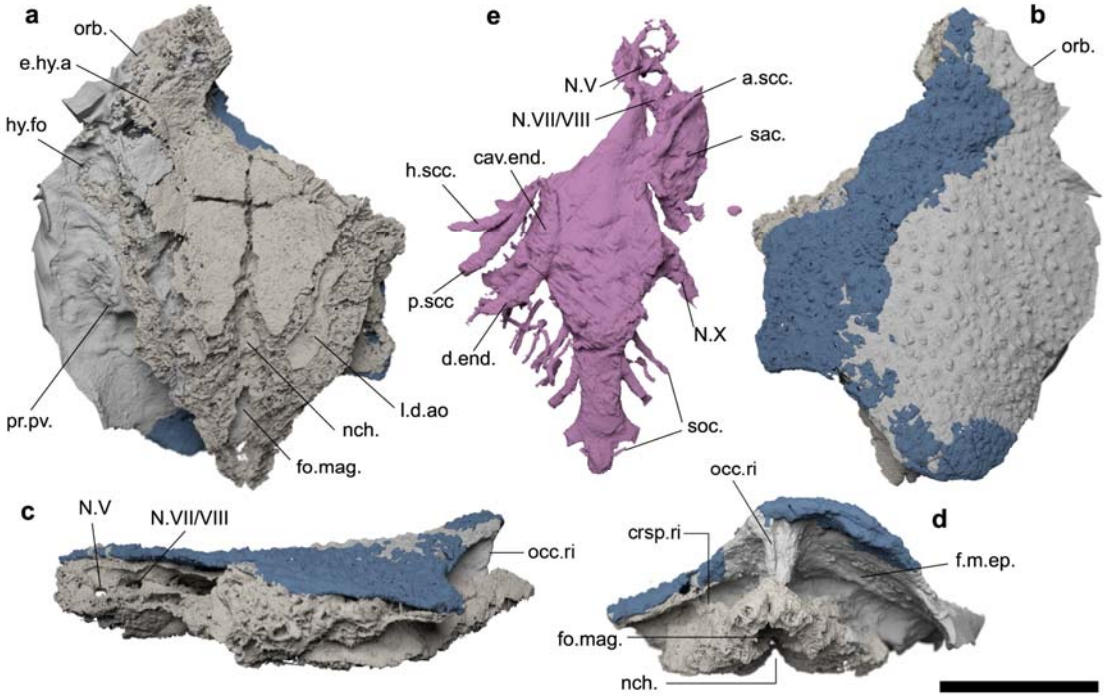

Fig. 1 | MPC-FH100/9.1 a 'placoderm' skull roof and braincase from the Early Devonian of Mongolia. a, Ventral view. **b**, Dorsal view. **c**, Left lateral view. **d**, Posterior view. **e**, Braincase endocavity in dorsal view. Taupe: endoskeleton; grey: mould; pink: endocavity; blue: exoskeleton. a.scc., anterior semicircular canal; cav.end., endolymphatic cavity; crsp.ri, craniospinal ridge; d.end., endolymphatic duct; e.hy.a., sulcus for the efferent hyoid artery; f.m.ep., epaxial muscle fossa; fo.mag., foramen magnum; h.scc., horizontal semicicular canal; l.d.ao, sulcus for the lateral dorsal aorta; N.V, trigeminal nerve canal; N.VII, facial nerve canal; N.VIII, acoustic nerve canal; N.X, vagus nerve canal; nch., notochordal canal; occ.ri, occipital ridge; orb., orbit; p.scc, posterior semicircular canal; pr.pv., paravagal process; sac., sacculus; soc., spino-occipital nerve canals. Scale bar, 20 mm.

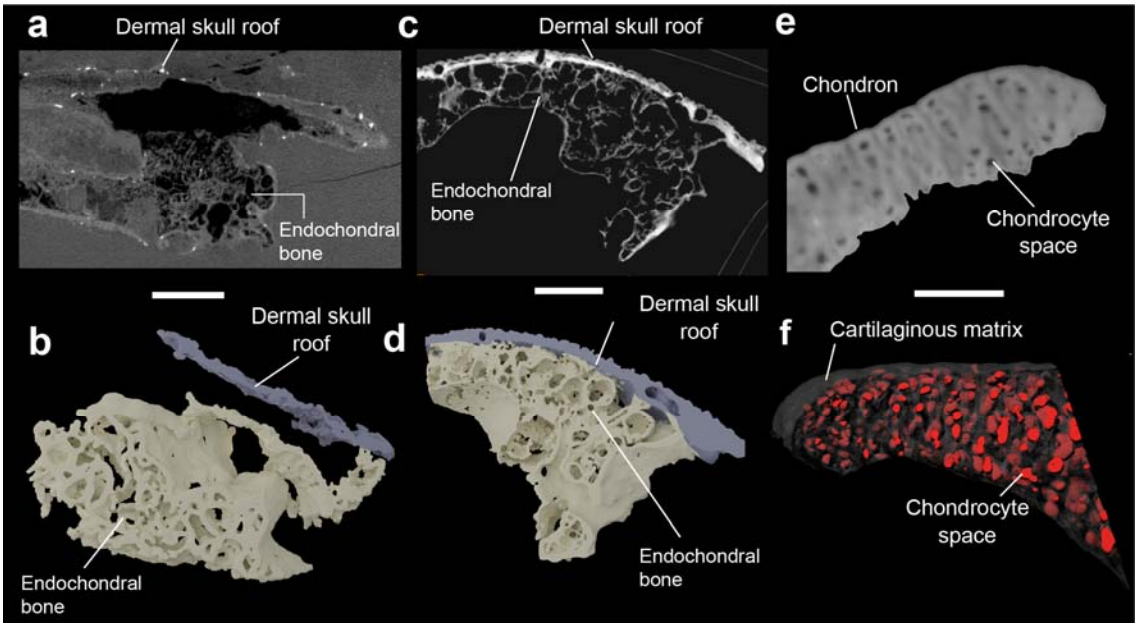

Fig. 2 | Endoskeletal mineralisation in fossil gnathostomes. a, Transverse tomographic slice through MPC-FH100/9.1. **b**, Three-dimensional rendering of trabecular bone structure. **c**, Transverse tomographic section through the braincase of the osteichthyan *Ligulalepis*. **d**, Three-dimensional rendering of the trabecular bone in *Ligulalepis* (**c** and **d** use data from[41]). **e**, Synchrotron tomography image of the calcified cartilage of the stem-group chondrichthyan *Diplacanthus crassisimus* specimen NMS 1891.92.334. **f**, Semi-transparent three-dimensional structure of calcified cartilage of NMS 1891.92.334. Scale bars, **a** and **b,** 10 mm; c and d, 1 mm ; **c** and **h**, 150 µm.

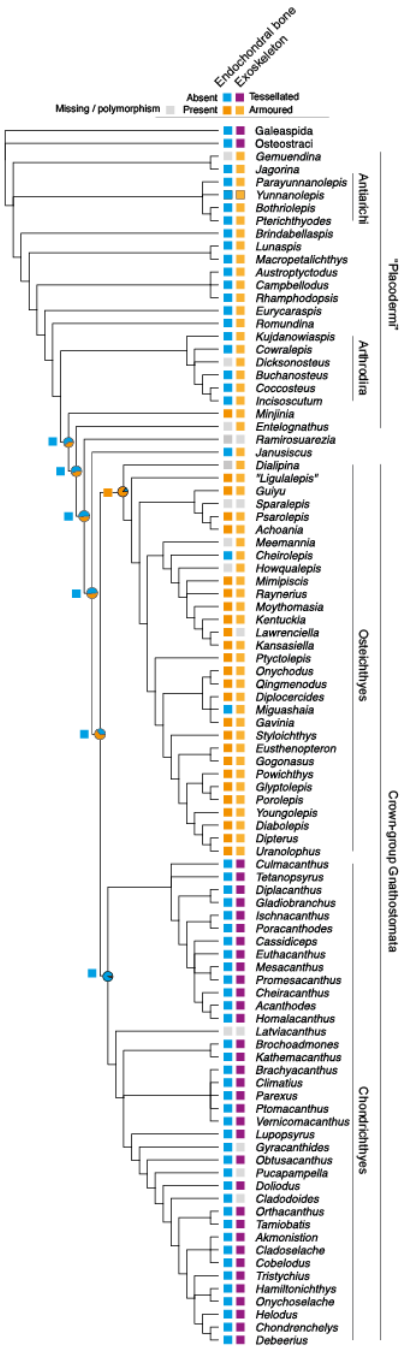

Fig. 3 | Summary phylogenetic relations of early gnathostomes showing distribution of endochondral bone and exoskeletal armour. Squares at nodes indicate parsimony reconstruction for endochondral bone. Pie charts at nodes show likelihood reconstructions for the same character under the all-rates-different model (see Extended Data Figs 6 & 7 for competing reconstructions). Grey box indicates uncertainty. Loss of endochondral bone maps closely with generalised loss of bone in chondrichthyans where exoskeletal armour and perichondral bone are also absent.

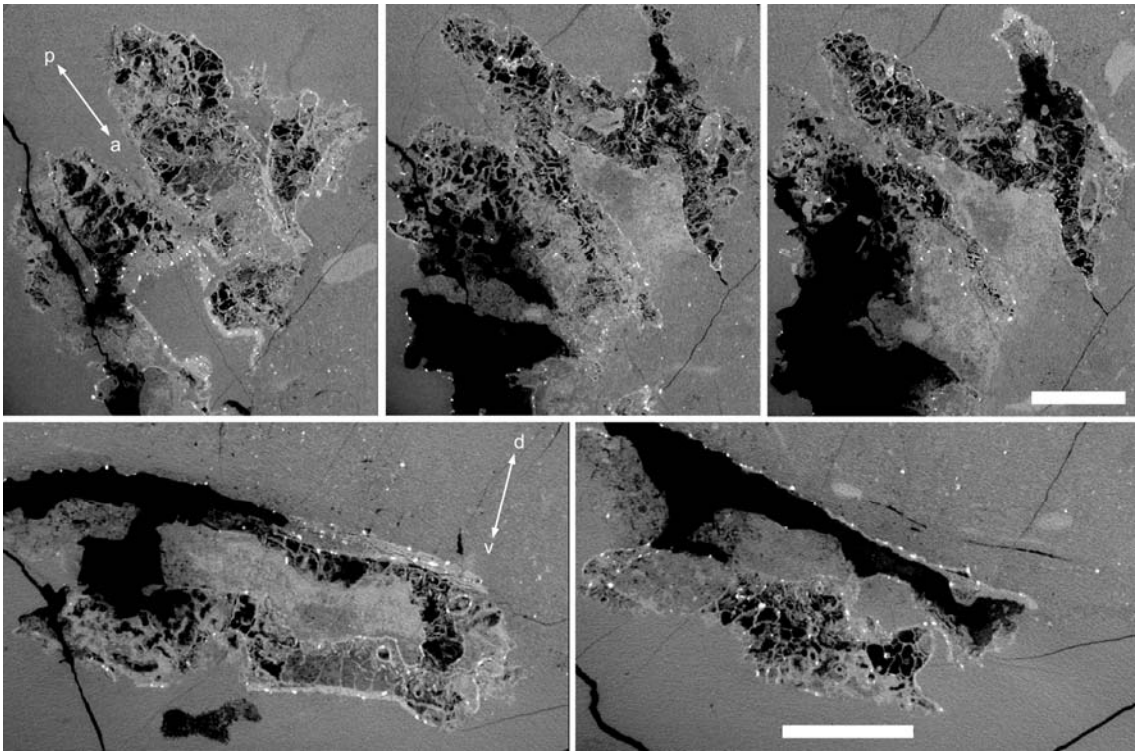

Extended Data Fig. 1 | Tomograms of endoskeletal ossification in *Minjinia*. Top row: semi-coronal sections through braincase. Double-headed arrows indicate anterior-posterior (a-p) dorsal-ventral (d-v) axes. Bottom row: semi-transverse sections through posterior part of endocranium. Voids of black space represent mouldic preservation. Scale bars, 10 mm and apply across each row of panels.

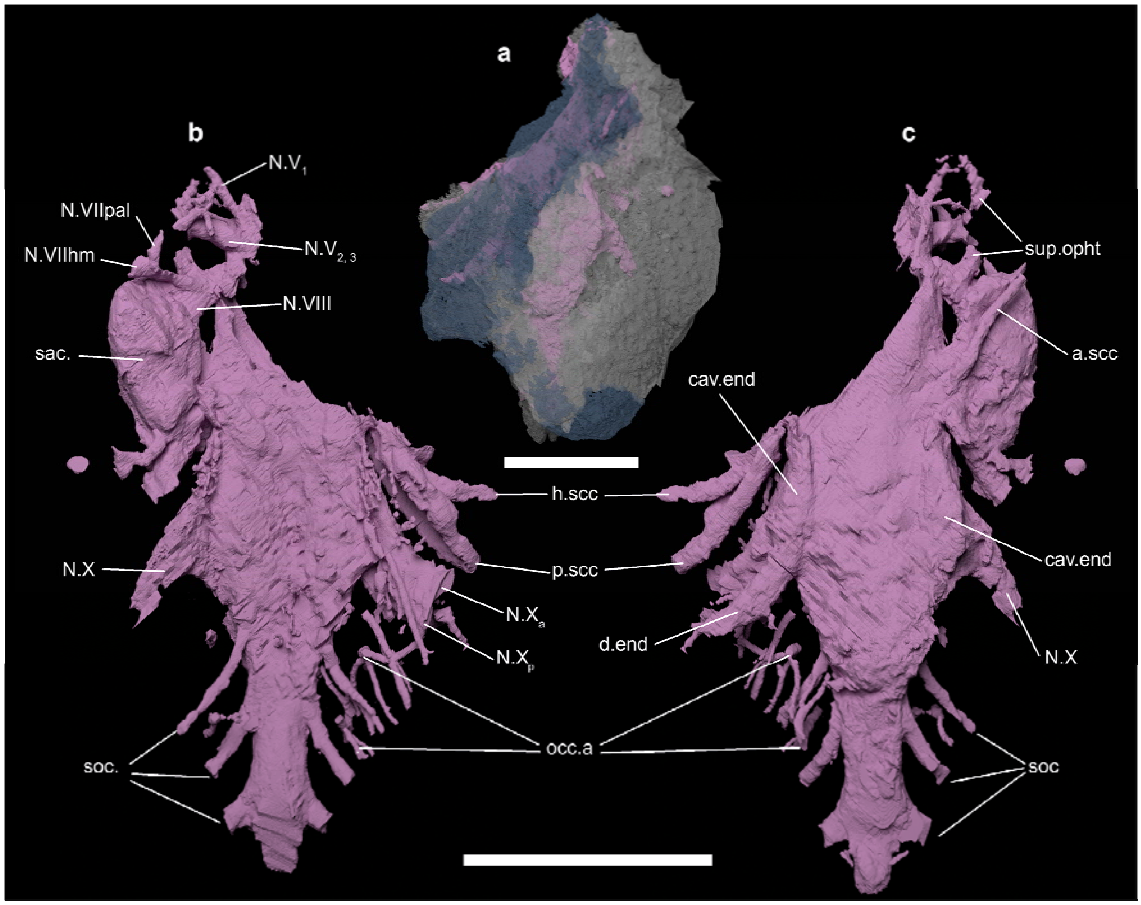

Extended Data Fig. 2 | Braincase endocavity of *Minjinia*. a, Semi-transparent rendering of skull roof and braincase (grey and blue) showing extent of endocavity (pink). **b,** Ventral view. **c,** Dorsal view. a.scc., anterior semicircular canal; cav.end., endolymphatic cavity; d.end., endolymphatic duct; h.scc., horizontal semicicular canal; l.d.ao., sulcus for the lateral dorsal aorta; N.V, trigeminal nerve canal; N.VIIhm, hyomandibular branch of facial nerve canal; N.VIIpal, palatine branch of facial nerve canal; N.VIII, acoustic nerve canal; N.X, vagus nerve canal, $N.X_a$, anterior branch of vagus nerve canal; N.Xp, posterior branch of vagus nerve canal; occ.a, occipital artery canals; p.scc, posterior semicircular canal; sac., sacculus; soc., spino-occipital nerve canals; sup.opth, canal for supra-ophtalmic nerve. Scale bars, 20 mm (upper scale bar associates with **a**, lower scale bar associates with **b** and **c**).

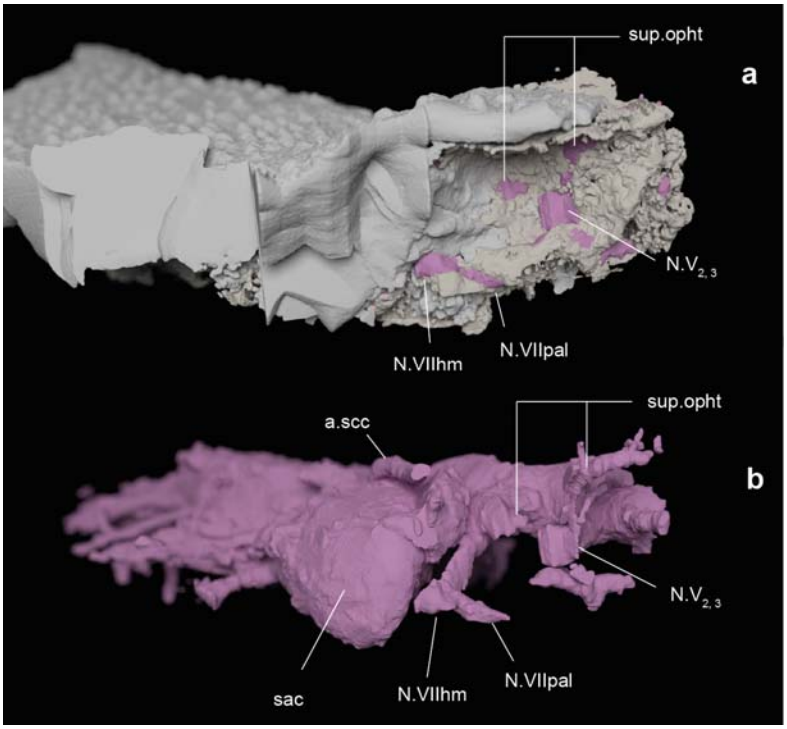

Extended Data Fig. 3 | Right orbital wall and innervation pattern of *Minjinia*. a, orbit in anterolateral view showing disposition of nerve openings (pink infill). **b**, endocast in the same perspective showing the relationship between never canals and endocast.

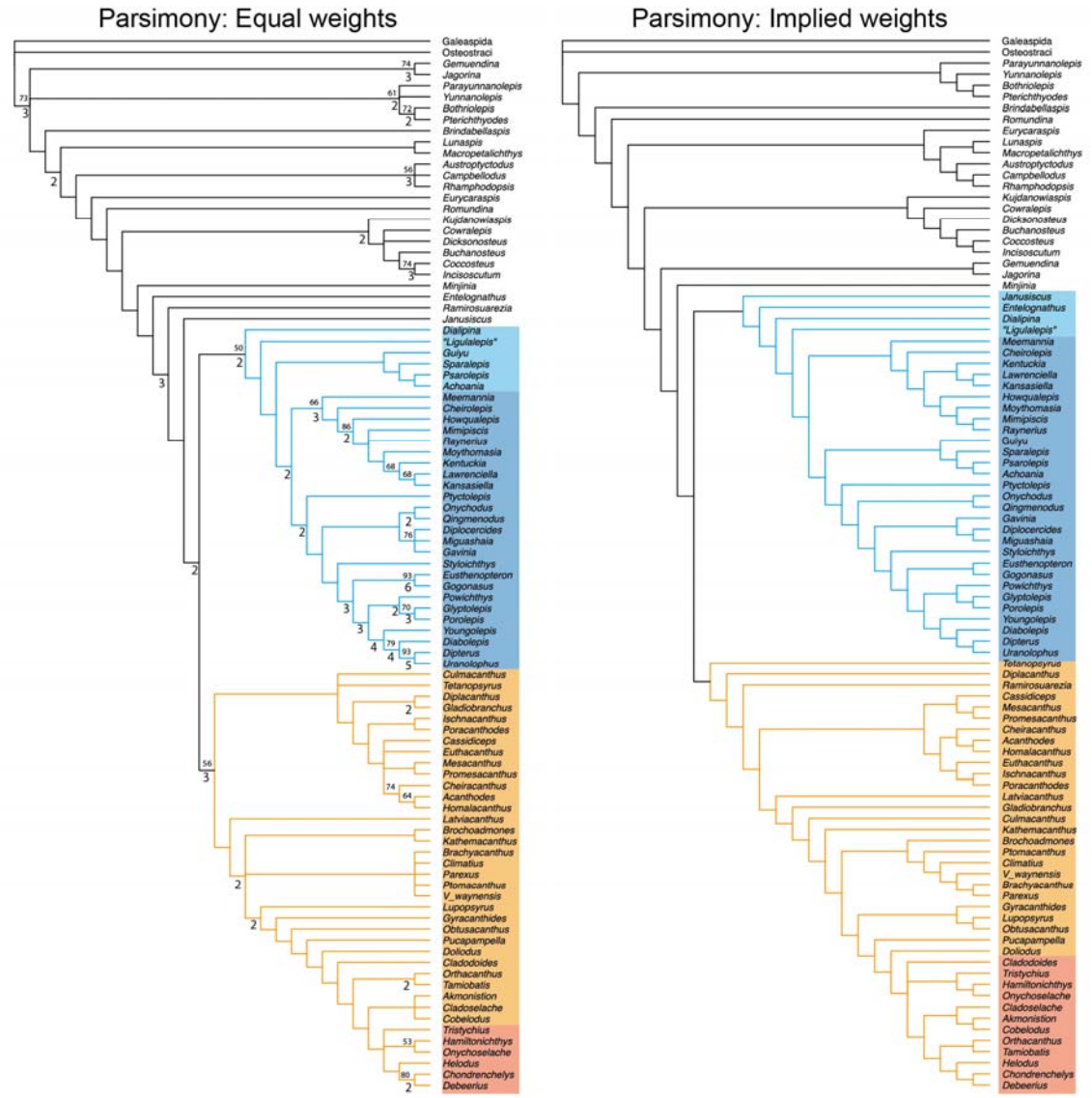

Extended Data Fig. 4 | Results of phylogenetic parsimony analysis. Dataset consists of 95 taxa and 284 characters. Both trees are strict consensus topologies. Equal weights parsimony analysis using the ratchet resulted in 240 trees with a length of 832 steps. Implied weights parsimony analysis using random addition sequence + branch-swapping resulted in two optimal trees with score 85.23240. Double-digit figures above internal branches are bootstrap values of 50% and over; single-digit figures below branches are Bremer decay index values. Blue shading: osteichthyan total group (dark blue: crown group); orange shading: chondrichthyan total group (dark orange: crown group).

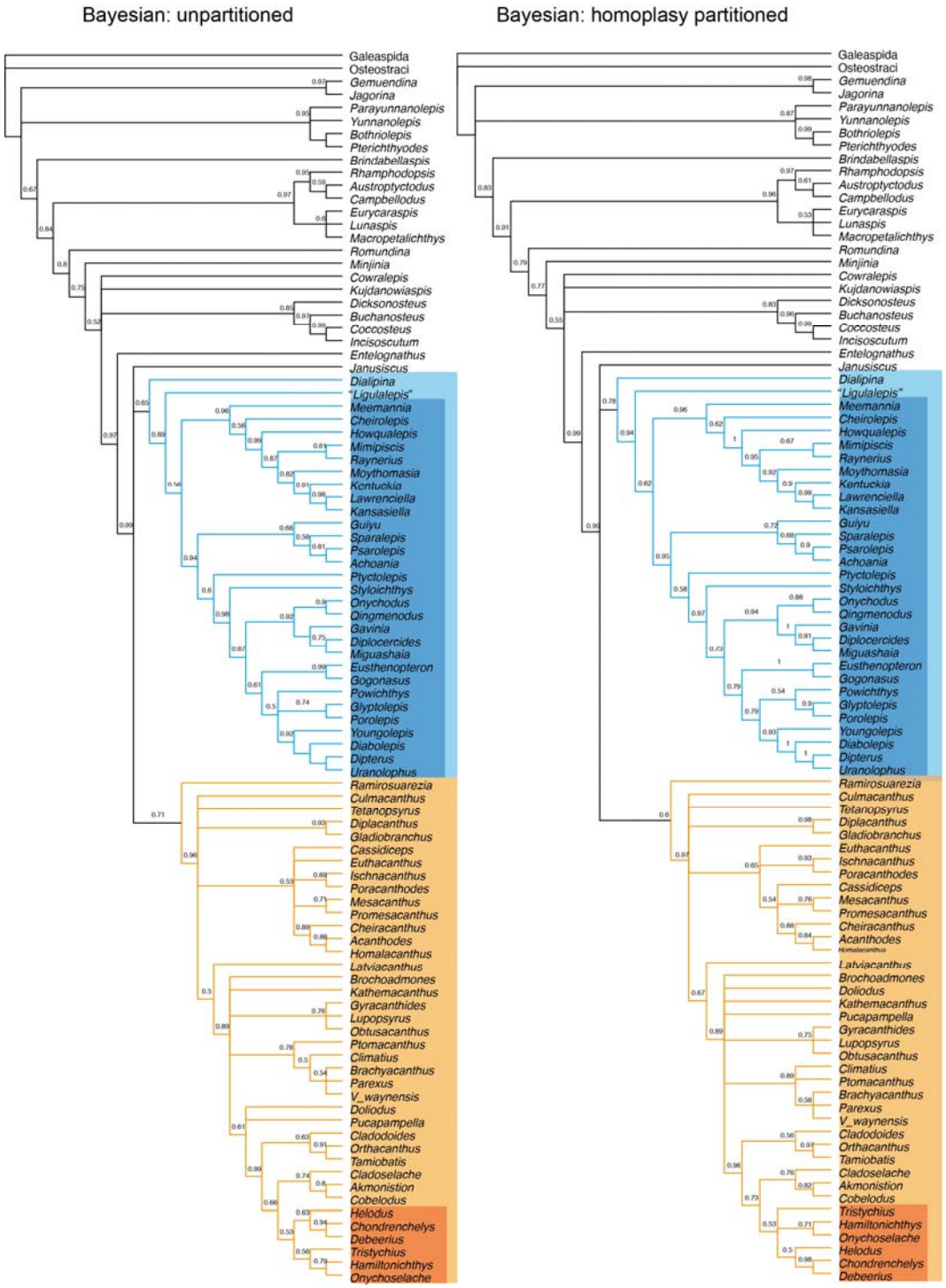

412

413 **Extended Data Fig. 5 | Results of Bayesian phylogenetic analysis using both partitioned**
414 **and unpartitioned data.** Majority-rules consensus trees with posterior probabilities shown
415 along branches. Blue shading: osteichthyan total group (dark blue: crown group); orange
416 shading: chondrichthyan total group (dark orange: crown group).

417

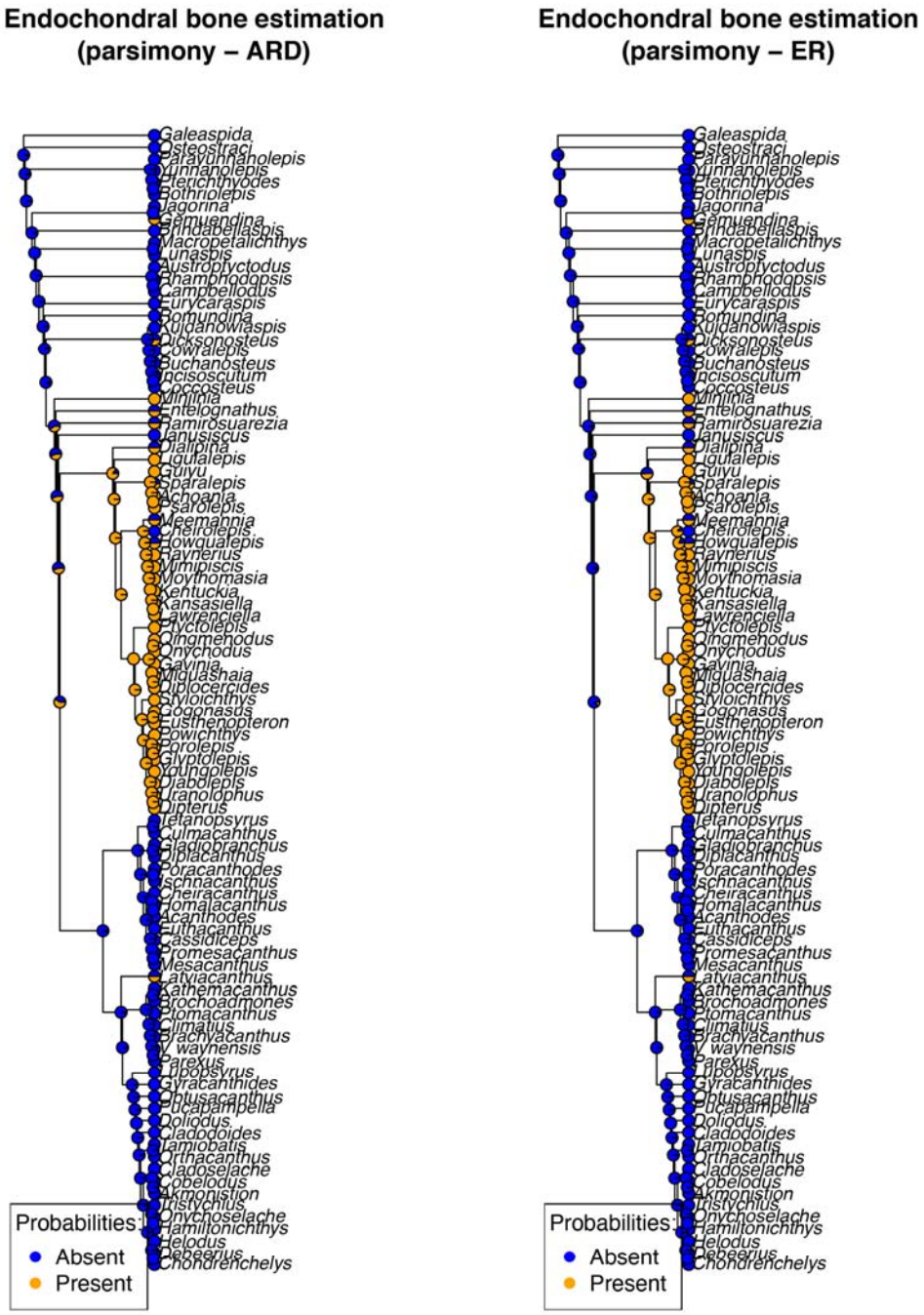

418

419 **Extended Data Fig. 6 | Likelihood ancestral state mapping of endochondral bone on**

420 **equal weights parsimony results.** ARD, all rates different model; ER, equal rates model.

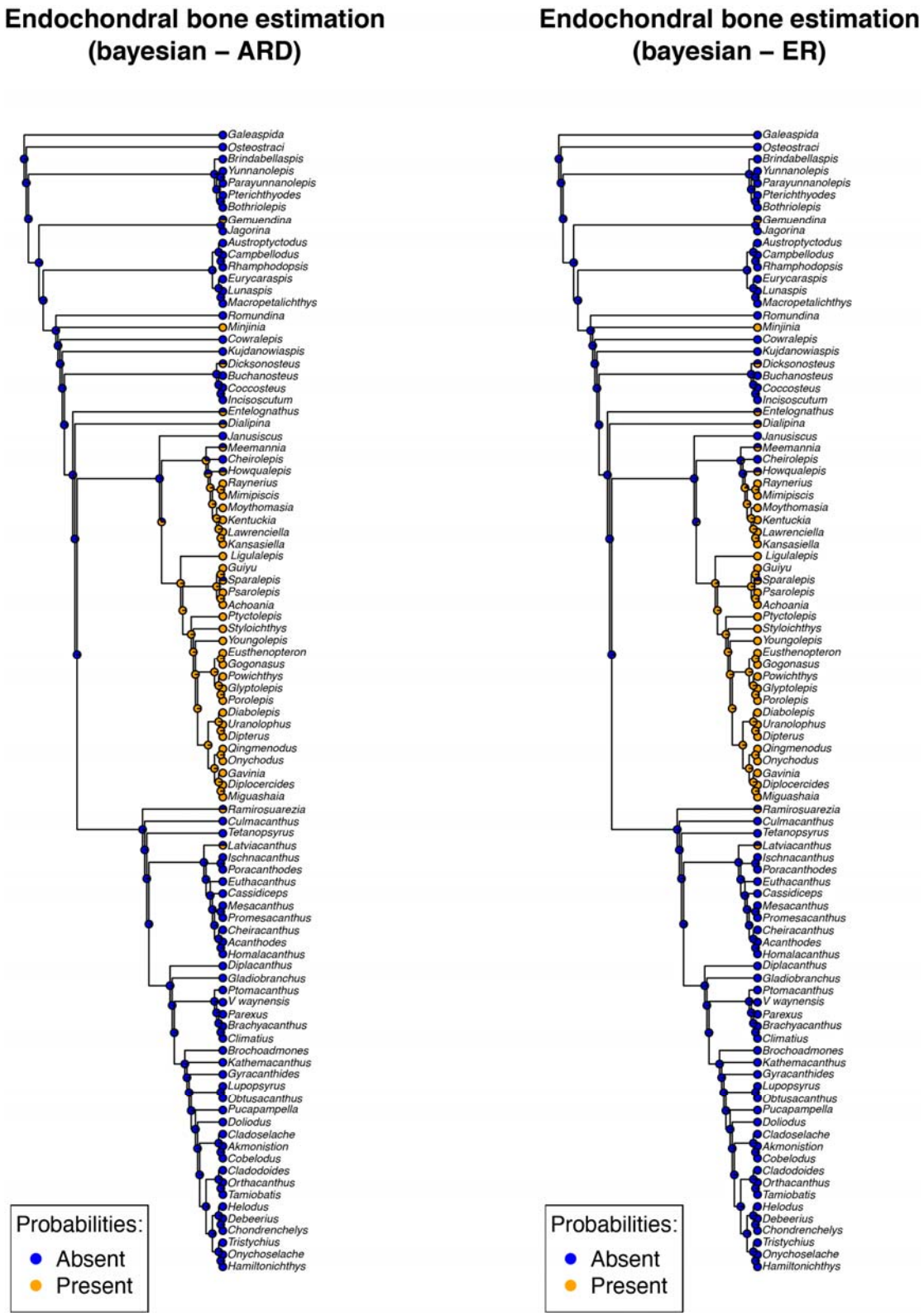

Extended Data Fig. 7 | Likelihood ancestral state mapping of endochondral bone on unpartitioned Bayesian analysis results. ARD, all rates different model; ER, equal rates model.

Extended Data Table 1 | Tree distribution (100) ancestral states estimation results. ER = Equal rates model; ARD = All Rates Different model. The columns AIC and log.lik represent the median AIC and log.lik across the 100 parsimony and bayesian trees (for both models). The columns Absent and Present represent the median scaled likelihood for the endochondral bone state.

Node	Tree	Model	log.lik	AIC	Absent	Present
Minjinia:crown gnathostomes	Parsimony	ER	-27.60	57.20	0.94	0.06
		ARD	-25.47	54.93	0.61	0.39
	Bayesian	ER	-29.94	61.89	0.98	0.02
		ARD	-27.69	59.38	0.82	0.18

References

1. Hall, B. K. *Bones and Cartilage*. (Academic Press, 2005).
2. Janvier, P. *Early Vertebrates*. (Oxford University Press, 1996).
3. Friedman, M. & Brazeau, M. A Reappraisal of the Origin and Basal Radiation of the Osteichthyes. *J Vertebr Paleontol* **30,** 36–56 (2010).
4. Brazeau, M. D. & Friedman, M. The characters of Palaeozoic jawed vertebrates. *Zool J Linn Soc* **170,** 779–821 (2014).
5. Eames, B. F. *et al.* Skeletogenesis in the swell shark Cephaloscyllium ventriosum. *Journal of Anatomy* **210,** 542–554 (2007).
6. Marconi, A., Hancock-Ronemus, A. & Gillis, J. A. Adult chondrogenesis and spontaneous cartilage repair in the skate, *Leucoraja erinacea*. *eLife Sciences* **9,** 2813 (2020).
7. Maisey, J. G. Heads and tails: a chordate phylogeny. *Cladistics* **2,** 201–256 (1986).
8. Zhu, M. Bone gain and loss: insights from genomes and fossils. *Natl Sci Rev* **1,** 490–492 (2014).
9. Alekseeva, R. E., Mendbayar, B. & Erlanger, O. A. *Brachiopods and Biostratigraphy of the Lower Devonian of Mongolia*. **16,** (Nauka, 1981).
10. Alekseeva, R. E. *Devonian Biostratigraphy of Mongolia*. (Nauka, 1993).
11. Mark-Kurik, E. in *Morphology, Phylogeny and Paleobiogeography of Fossil Fishes* (eds. Elliott, D. K., Maisey, J., Yu, X. & Miao, D.) 101–106 (2010).
12. Stensiö, E. A. Contributions to the knowledge of the vertebrate fauna of the Silurian and Devonian of western Podolia. II. Notes on two arthrodires from the Downtonian of Podolia. **35A,** 1–83 (1944).
13. Ørvig, T. Description, with special reference to the dermal skeleton, of a new radotinid arthrodire from the Gedinnian of Arctic Canada. *Colloque international C.N.R.S. no. 218* 43–71 (1975).
14. Vaškaninová, V. & Ahlberg, P. E. Unique diversity of acanthothoracid placoderms (basal jawed vertebrates) in the Early Devonian of the Prague Basin, Czech Republic: A new look at Radotina and Holopetalichthys. *PLoS ONE* **12,** e0174794 (2017).

15. Wängsjö, G. The Downtonian and Devonian vertebrates of Spitsbergen. IX. *Norsk Polarinstitutt Skrifter* **97,** 1–611 (1952).
16. Charest, F., Johanson, Z. & Cloutier, R. Loss in the making: absence of pelvic fins and presence of paedomorphic pelvic girdles in a Late Devonian antiarch placoderm (jawed stem-gnathostome). *Biology Letters* **14,** 20180199 (2018).
17. Dupret, V., Sanchez, S., Goujet, D. & Ahlberg, P. E. The internal cranial anatomy of *Romundina stellina* Ørvig, 1975 (Vertebrata, Placodermi, Acanthothoraci) and the origin of jawed vertebrates—Anatomical atlas of a primitive gnathostome. *PLoS ONE* **12,** e0171241 (2017).
18. Olive, S., Goujet, D., Lelièvre, H. & Janjou, D. A new Placoderm fish (Acanthothoraci) from the Early Devonian Jauf Formation (Saudi Arabia). *Geodiversitas* **33,** 393–409 (2011).
19. Stensiö, E. A. La cavité labyrinthique, l'ossification sclérotique et l'orbite de *Jagorina*. *Colloques internationaux du Centre national de la Recherche scientifique* **21,** 9–43 (1950).
20. Stensiö, E. A. Anatomical studies on the arthrodiran head. *K Sven Vetenskapsakad Handl* **9,** 1–419 (1963).
21. Goujet, D. *Les poissons placodermes du Spitsberg*. (Cahiers de Paléontologie, Editions du CNRS, 1984).
22. Davis, S. P., Finarelli, J. A. & Coates, M. I. *Acanthodes* and shark-like conditions in the last common ancestor of modern gnathostomes. *Nature* **486,** 247–250 (2012).
23. Castiello, M. & Brazeau, M. D. Neurocranial anatomy of the petalichthyid placoderm *Shearsbyaspis oepiki* Young revealed by X□ray computed microtomography. *Palaeontology* **21,** 754 (2018).
24. Rosa, B. B., Melo, G. A. R. & Barbeitos, M. S. Homoplasy-Based Partitioning Outperforms Alternatives in Bayesian Analysis of Discrete Morphological Data. *Systematic Biology* **54,** 373 (2019).
25. Rosen, D. E., Forey, P. L., Gardiner, B. G. & Patterson, C. Lungfishes, tetrapods, paleontology, and plesiomorphy. *Bull Am Mus Nat Hist* **167,** 159–276 (1981).
26. Gardiner, B. G. The relationships of the palaeoniscid fishes, a review based on new specimens of *Mimia* and *Moythomasia* from Upper Devonian of Western Australia. *Bull Br Mus nat Hist (Geol)* **37,** 173–428 (1984).
27. Zhu, M. *et al.* A Silurian placoderm with osteichthyan-like marginal jaw bones. *Nature* **502,** 188–193 (2013).
28. Giles, S., Friedman, M. & Brazeau, M. D. Osteichthyan-like cranial conditions in an Early Devonian stem gnathostome. *Nature* **520,** 82–85 (2015).
29. Miles, R. S. in *Interrelationships of Fishes* (eds. Greenwood, P. H., Miles, R. S. & Patterson, C.) 63–103 (Academic Press London, 1973).
30. Janvier, P. *Les céphalaspides du Spitsberg*. (Éditions du Centre National de la Recherche Scientifique, 1985).
31. Young, G. C. New information on the structure and relationships of *Buchanosteus* (Placodermi: Euarthrodira) from the Early Devonian of New South Wales. *Zool J Linn Soc* **66,** 309–352 (1979).
32. Stensiö, E. A. On the head of the macropetalichthyids. *Field Museum of Natural History Publication Geological Series* **4,** 87–197 (1925).
33. Ørvig, T. Notes on some Paleozoic lower vertebrates from Spitsbergen and North America. *Norsk Geologisk Tidsskrift* **37,** 285–353 (1957).
34. Schaeffer, B. The braincase of the holostean fish *Macrepistius*, with comments on neurocranial ossification in the Actinopterygii. *American Museum Novitates* **2459,** 1–34 (1971).

35. Cloutier, R. in *Devonian Fishes and Plants* (eds. Schultze, H.-P. & Cloutier, R.) 227–247 (Verlag Dr. Friedrich Pfeil, 1996).
36. Grande, L. & Bemis, W. E. Osteology and Phylogenetic Relationships of Fossil and Recent Paddlefishes (Polyodontidae) with Comments on the Interrelationships of Acipenseriformes. *Memoir (Society of Vertebrate Paleontology)* **11 (Supplement to Number 1),** 1–121 (1991).
37. Venkatesh, B. *et al.* Elephant shark genome provides unique insights into gnathostome evolution. *Nature* **505,** 174–179 (2014).
38. Ryll, B., Sanchez, S., Haitina, T., Tafforeau, P. & Ahlberg, P. E. The genome of *Callorhinchus* and the fossil record: a new perspective on SCPP gene evolution in gnathostomes. *Evolution & Development* **16,** 123–124 (2014).
39. Goloboff, P. A. & Catalano, S. A. TNT version 1.5, including a full implementation of phylogenetic morphometrics. *Cladistics* **32,** 221–238 (2016).
40. Ronquist, F. & Huelsenbeck, J. P. MrBayes 3: Bayesian phylogenetic inference under mixed models. *Bioinformatics* **19,** 1572–1574 (2003).
41. Clement, A. M. *et al.* Neurocranial anatomy of an enigmatic Early Devonian fish sheds light on early osteichthyan evolution. *eLife Sciences* **7,** e34349 (2018).
42. Lewis, P. O. A likelihood approach to estimating phylogeny from discrete morphological character data. *Systematic Biology* **50,** 913 (2001).
43. Rambaut, A., Drummond, A. J., Xie, D., Baele, G. & Suchard, M. A. Posterior Summarization in Bayesian Phylogenetics Using Tracer 1.7. *Systematic Biology* **67,** 901–904 (2018).
44. R Core Team. *R: A language and environment for statistical computing.* (R Foundation for Statistical Computing, 2019).
45. Maddison, D. R. & Maddison, W. P. *Mesquite*. (2019).
46. Louca, S. & Doebeli, M. Efficient comparative phylogenetics on large trees. *Bioinformatics* **34,** 1053–1055 (2017).
47. Swofford, D. L. *PAUP**. 4.0a166, (2019).